Atmospheric Profiling of Water Vapor Density with a 20.5–23.5 GHz Autocorrelation Radiometer

CHRISTOPHER S. RUF AND CALVIN T. SWIFT

The Microwave Remote Sensing Laboratory, Department of Electrical and Computer Engineering, University of Massachusetts, Amherst, Massachusetts

(Manuscript received 21 July 1987, in final form 11 January 1988)

ABSTRACT

A tropospheric water vapor density profiling system is presented. The hardware consists of an autocorrelation radiometer (CORRAD) operating over a frequency range from 20.5 to 23.5 GHz. The CORRAD directly measures the autocorrelation of downwelling thermal emission from the atmosphere. The 3 GHz predetection bandwidth of each measurement provides for extremely rapid decorrelation of the noise inherent in all radiometer measurements. This, in turn, allows for high temporal resolution of the water vapor dynamics. Fourier transformation of the raw data produces a brightness temperature spectrum with 100 MHz resolution across the frequency range. Inversion of the radiative transfer integral equation to solve for the water vapor distribution is constrained by the 31 equivalent frequency channels. Previous microwave profilers of the troposphere, with 2 to 5 frequency channels, were much less constrained and the inversion process was accordingly more sensitive to measurement noise. Water vapor profiles estimated by the inversion are in good agreement with coincident radiosonde measurements made by the National Weather Service.

1. Introduction

Water vapor is one of the most dynamic variables in the atmosphere. Obtaining real time information about its magnitude and distribution in the troposphere is an important problem in the meteorological sciences. Radiosonde balloon profiles of the atmosphere constitute a useful, but limited, sampling of the water vapor. Balloon datasets are point measurements made along the line of ascension of the sensor. That line varies with the winds, and point measurements are only an approximation of the volume averaged information pertinent to meteorological predictions or modeling. Furthermore, frequent balloon launchings are expensive and difficult to coordinate in an operational setting. Microwave radiometry offers a clear alternative to the radiosonde balloon for certain aspects of atmospheric sounding. This technique can provide highly repeatable measurements of the water vapor profile in the air, averaged over a controlled volume of space and recorded continuously without any user interaction. The basis for radiometric profiling lies in the thermal emission characteristics of the atmosphere. Near the 22.235 GHz water vapor absorption line, the part of the thermal emission due to water vapor which is measured by an upward looking radiometer can be approximated by

$$T_B(f) = \int_0^\infty W(f, h)\rho_v(h)dh \qquad (1)$$

where $T_B(f)$ is the brightness temperature of the emission (in K) at a frequency f, $\rho_v(h)$ is the water vapor density in the atmosphere (in g/m^3) at a height h, and $W(f, h)$ is the weighting function provided by a linearization of the equation of radiative transfer.

The exact form of the integral weighting function, $W(f, h)$, is discussed in the literature (Benoit, 1968). This attention has focused primarily on the line shape of the pressure broadened absorption spectrum underlying the weighting function. The weighting function is derived by a first order Taylor expansion of the full, nonlinear equation of radiative transfer. The expansion is performed around a typical water vapor profile. The exact shape of the weighting function, then, is determined by all the variables comprising the equation of radiative transfer. The spectrum of the atmospheric absorption (line shape) is one of these variables. Another is the altitude profile of the air temperature. The effects of errors in any particular line shape on the quality of the water vapor profile estimates is very small because 1) the various possible line shapes addressed in the literature have significant differences only away from the line center (22.235 GHz) near which CORRAD operates, and 2) the system calibration procedure used on the CORRAD raw data employs the same line shape function as the profile inversion procedure for internal consistency. This calibration procedure is described more fully in section 5. Deviations of the true

Corresponding author address: Dr. Christopher S. Ruf, Dept. of Electrical and Computer Engineering, The University of Massachusetts, Amherst, MA 01003.

air temperature profile from the profile which is assumed in order to generate the weighting function also have a relatively small effect on the quality of the water vapor profile estimate. This results from the weak absorption characteristic near 22.235 GHz. Because the absorption is weak, the atmosphere's thermal emission is considerably lower (typically by a factor of 5–10) than its physical temperature. The effects of errors in the assumed physical temperature on the measured thermal emission are reduced by the same factor.

The weighting function used here is summarized by Ulaby et al. (1981 and 1986) and is plotted in normalized form for several frequencies, as in Fig. 1. The figure plots the contribution made by water vapor to the measured brightness temperature versus height, normalized to a maximum contribution of unity at the altitude appropriate for each frequency. Frequencies closest to the 22.235 GHz resonance are most sensitive to the water vapor at higher altitudes. Samples of the brightness temperature at different frequencies near resonance allow the integral relation given by (1) to be inverted with respect to the water vapor profile.

2. Available radiometer technology

Samples of the brightness temperature spectrum near 22.235 GHz can be made in several ways. The most common sampling schemes have been designed around the total power radiometer (Decker et al. 1978; Askne and Skoog 1983). These systems feature a parallel bank of channels, one channel for each frequency. Additional gain stabilization techniques are often employed in order to reduce the effects of hardware drift between calibrations. Examples of these techniques include Dicke switching (Dicke 1946) and feedback nulling (Groggins 1967). However, while certain details of calibration differentiate these radiometers, the approach used to sample different frequency bins places all of them in a common class with the total power radiometer. The size and cost of the independent channels which are required severely restricts the number of frequencies sampled. Typical profilers of this type provide, at most, five samples of the brightness temperature spectrum.

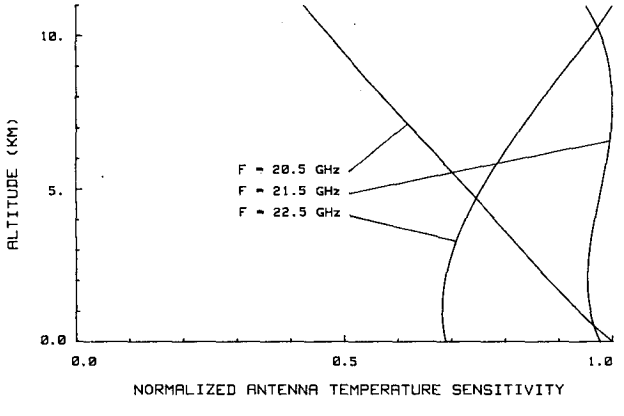

FIG. 1. Normalized profile inversion weighting functions. The brightness temperature measured by an upward looking radiometer is sensitive to the water vapor density at all altitudes. The variation in sensitivity with altitude is different for different frequency channels. Measurements at a number of frequencies can be inverted to recover the vertical profile of the water vapor.

One alternative method of spectral sampling is the stepped frequency radiometer (Jones et al. 1981). The frequency component of interest at the antenna is mixed down to a constant intermediate lower frequency by multiplication with a variable local oscillator frequency. In this way, different input frequency components can be sampled without the need for independent channels. The number of samples possible is limited only by the bandwidth performance of the front end hardware.

Microwave autocorrelation radiometry performs the necessary spectral measurements through a synthesis of techniques developed for correlation radiometry and optical Fourier transform spectroscopy. Correlation radiometers are most commonly used to cross-correlate spatially separated radio telescopes for interferometric synthetic aperture imaging (Kraus 1966). They perform the multiplication and expectation operations required of a cross correlator on two broadband signals. Optical Fourier transform spectroscopy determines the power spectral density of a signal in the optical frequency range indirectly, by measuring its autocorrelation function. In general, the autocorrelation, $R_x(\tau)$, and power spectral density, $S_x(f)$, of a complex, wide-sense stationary random process, $x(t)$, are related by (Papoulis 1984):

$$R_x(\tau) = \langle x^*(t)x(t+\tau)\rangle \tag{2}$$

$$S_x(f) = \int_{-\infty}^{\infty} R_x(\tau)e^{-j2\pi f\tau}d\tau \tag{3}$$

where $\langle \cdot \rangle$ denotes the expectation operator and $*$ denotes complex conjugation.

In the case of an upward looking radiometer, $x(t)$ is identified as the voltage time series at the antenna terminals corresponding to a downwelling brightness temperature spectrum $T_B(f)$ from the atmosphere. This spectrum is related to the power spectral density by

$$T_B(f) = \begin{cases} \dfrac{2}{kZ_0}S_x(f), & f \geq 0 \\ 0, & \text{otherwise} \end{cases} \tag{4}$$

where k is Boltzmann's constant $\approx 1.38 \times 10^{-23}$W K^{-1} Hz^{-1} and Z_0 is the characteristic impedance at the antenna terminals. Equations (2)–(4) imply that a microwave autocorrelation ratiometer will produce samples of the brightness temperature spectrum by a Fourier transformation of measurements of the cross-correlation of a signal with a time-delayed version of itself.

Several early versions of the autocorrelation radiometer were built and operated as proof-of-concept tests which, although successful, apparently did not develop into working remote sensing systems (Page et al. 1953; Vecchio 1965). This was probably due to their low operating frequencies (150 MHz and 1.1 GHz) and to the underdeveloped state of radiometric remote sensing at the time of their development. More recently, a very narrowband (6.67 MHz) autocorrelation radiometer has been used to profile water vapor in the upper stratosphere and mesosphere (Thacker et al. 1981). The signal-to-noise problems associated with this sensor necessitated integration times on the order of a day, thus obscuring any short term temporal dynamics. In addition, this profiler lacked sensitivity to the water vapor below about 45 km altitude.

3. Radiometer technology comparison

The advantage of an autocorrelation approach to spectral imaging lies in the bandwidth, B, and integration time, T, available for each measurement. The signal-to-noise (SNR) performance of most radiometers (ratio of the mean to the standard deviation of the measured system brightness temperature) is given by

$$\mathrm{SNR} = K(BT)^{1/2} \tag{5}$$

where $K \approx 1$ is proportionality constant determined by the radiometer hardware specifics. The bandwidth and integration time available for the three radiometer systems discussed above, and the resulting SNR performance, is summarized in Table 1 for the case of a total frequency range B_{TOT} which is to be resolved into N adjacent frequency bins during a time T_{TOT}.

In Table 1, the worst case performance by the autocorrelation radiometer (with serial time delay sampling) is as good as a bank of N total power radiometers and better than the single-stepped frequency radiometer. This advantage should be qualified, however, by noting that the Fourier transformation required to recover the brightness temperature spectrum from the autocorrelation measurements degrades the SNR of the transformed data by $N^{-1/2}$ relative to the original data (Ruf 1987). This degradation can be viewed as a root-sum-squared accumulation of measurement noise during data processing. The discrete Fourier transformation at each frequency is a weighted linear combination of the individual data points. If the measurement noise associated with each point is modeled as independent additive Gaussian noise, then the standard deviation of the linear combination is the weighted root-sum-square of the individual standard deviations.

If the brightness temperature is the desired end product of the measurements, then the performance of the autocorrelation radiometer becomes comparable to that of the stepped frequency radiometer if its time delays are sampled serially and are comparable to the total power radiometer bank if they are sampled in parallel. Preliminary investigations into a formulation of the integral inversion problem with respect to the autocorrelation function [i.e., the Fourier transformation of (1)] suggest that the degrading transformation from measured autocorrelation samples to derived brightness temperature spectrum may be avoidable. Such a formulation could recover the SNR advantage possible with an autocorrelation radiometer.

4. The CORRAD sensor

A K-Band Autocorrelation Radiometer (CORRAD) was built by The Microwave Remote Sensing Laboratory at the University of Massachusetts at Amherst. The sensor is described schematically by Fig. 2 and pertinent operating specifications are summarized in Table 2. The CORRAD is of the serial delay line type and is therefore characterized by a relative SNR of its brightness temperature spectrum of N^{-1}.

The input signal at the antenna is first split by introducing it into the Σ-Arm of a waveguide magic-T. The two signals are next mixed down to an intermediate frequency (IF) bandpass of 4.5 to 7.5 GHz by two local oscillators which are phase-locked at 16.00 and 16.03 GHz. One of the IF branches is then run through a variable length of nondispersive transmission line (coax) to generate the necessary time delays. The two signals are then recombined and squared by a high-

TABLE 1. Radiometer SNR comparison.

			Autocorrelation	
	Total power	Stepped frequency	Parallel*	Serial†
Bandwidth (B)	B_{TOT}/N	B_{TOT}/N	B_{TOT}	B_{TOT}
Integration time (T)	T_{TOT}	T_{TOT}/N	T_{TOT}	T_{TOT}/N
Relative SNR of raw data‡	$N^{-1/2}$	N^{-1}	1	$N^{-1/2}$
Relative SNR of brightness temperature@ (after Fourier transform)	$N^{-1/2}$	N^{-1}	$N^{-1/2}$	N^{-1}

* All time-delay measurements were made simultaneously.
† Time delay measurements were made consecutively.
‡ $[(BY)/(B_{\mathrm{TOT}}T_{\mathrm{TOT}})]^{1/2}$.
@ Same as raw data for total power and stepped frequency radiometers $[(BT)/(NB_{\mathrm{TOT}}T_{\mathrm{TOT}})]^{1/2}$ for autocorrelation radiometers.

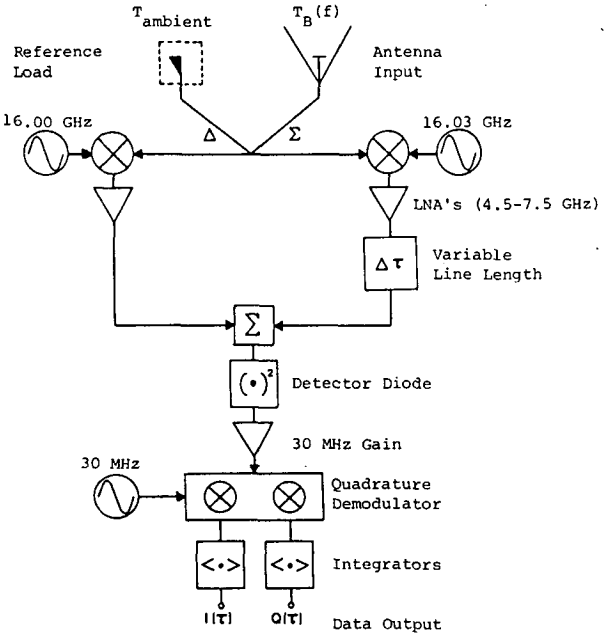

FIG. 2. CORRAD hardware schematic. The brightness temperature spectrum is determined indirectly, via measurements of the autocorrelation of the thermal noise. The autocorrelation is sampled by cross correlating the voltage time series at the antenna with a time delayed version of itself.

sensitivity detector diode. A cross-term is generated at 30 MHz which is proportional to the complex multiplication of the correlated portions of the two signals entering the first downconversion mixers (from 20.5–23.5 GHz to 4.5–7.5 GHz), except that a time delay has been added to one of the signals. Finally, the cross term is quadrature demodulated by a 30 MHz source which is phase-locked to the difference in frequency between the two original local oscillators, and the outputs are integrated to reduce the noise. This method of signal multiplication, which is known as sideband correlation, is used because of the very wide bandwidths involved.

The final data product, labeled $I(\tau)$ and $Q(\tau)$ in Fig. 2, can be described mathematically by

$$I(\tau) = \mathrm{Re}\{R_\gamma(\tau)\} \tag{6}$$

$$Q(\tau) = \mathrm{Im}\{R_\gamma(\tau)\} \tag{7}$$

where $\mathrm{Re}\{\cdot\}$ and $\mathrm{Im}\{\cdot\}$ denote real and imaginary components, respectively.

TABLE 2. CORRAD specifications.

RF bandpass	20.5–23.5 GHz
Time delays	−0.2–6.1 ns (0.1 ns steps)
Frequency resolution	160 MHz (null-to-null)/100 MHz (3 dB)
Receiver noise temp.	2000 K
Noise floor (ΔT)	0.5 K/sec$^{1/2}$

$$R_\gamma(\tau) = \int_{-\infty}^{\infty} S_\gamma(f) e^{j2\pi f\tau} df \tag{8}$$

$$S_\gamma(f) = \begin{cases} 4S_x(f + 16\ \mathrm{GHz}), & f \geq 0 \\ 0, & \text{otherwise} \end{cases} \tag{9}$$

$$S_x(f) = \frac{kZ_0}{2} T_B(|f|) \tag{10}$$

A sample of the raw data produced by CORRAD is plotted in Fig. 3. Several identifying features of a "textbook" autocorrelation function are evident from the figure. The real part of the function should be even and the imaginary part should be odd. Deviations from this behavior are due to the slightly nonuniform spacing between the actual time delays. The function should oscillate with a period of $(6.0\ \mathrm{GHz})^{-1} = 0.17$ ns due to the carrier frequency implied by (9), and it appears to do so. Finally, the function should decay with τ, as do the plots.

The 0.1 ns steps between samples of the autocorrelation function satisfy the Nyquist sampling requirements of this system. The maximum frequency component of the sampled function is 7.5 GHz. This would ordinarily imply a step size of at most $(2 \times 7.5\ \mathrm{GHz})^{-1} = 0.067$ ns. However, the complex sampling scheme used here allows a corresponding quadrature sampling theorem to dictate the sampling requirements (Rice and Wu 1982). Quadrature samples need only be taken at half the conventional Nyquist rate. The 0.1 ns steps used here are a conservative fulfillment of the quadrature step size requirement of $(7.5\ \mathrm{GHz})^{-1} = 0.13$ ns.

5. Data calibration

The brightness temperature spectra derived from the data by Fourier transformation were calibrated against a series of simultaneous radiosonde balloon soundings

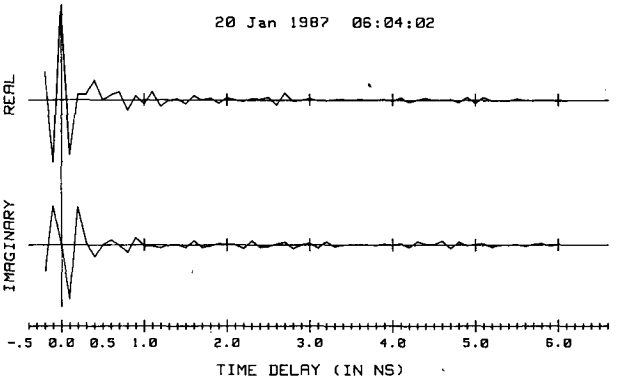

FIG. 3. Raw autocorrelation data. The time delay samples are varied from −0.2 to +6.1 ns in 0.1 ns steps. Note the Hermitian form of the measurements; the real part is even and the imaginary part is odd. This is consistent with the purely real brightness temperature spectrum.

by linear regression. The balloons were launched at 1800 EDT on 19 January 1987 and 0600 and 1800 EDT on 20 January 1987 in West Palm Beach, Florida. The temperature, pressure, and dewpoint profiles measured by the radiosonde were used to predict the downwelling brightness temperature spectrum between 20.5 and 23.5 GHz analytically, through the equation of radiative transfer. This prediction ranged from 60.2 K to 71.4 K at 22.2 GHz over the three soundings. Coincidently, with the balloon ascensions, autocorrelation measurements were made by CORRAD every 10 min. Three of these measurements were averaged together for each balloon launch to account for the ascension time of the balloon (approximately 30 min to 8 km altitude). The CORRAD measurements were Fourier transformed, producing an uncalibrated mean radiometer spectrum at each of the three launch times. These CORRAD spectra are, at this point, in raw "A/D" units. Data calibration is achieved by performing a least-squares linear regression on the raw data spectrum versus the predicted brightness temperature spectrum independently at each frequency. This provides slope and y-intercept spectra which can be applied to the individual raw spectra to produce a calibrated brightness temperature spectrum every 10 minutes. A sample of the calibrated spectrum is shown in Fig. 4, along with the corresponding spectrum predicted by theory from the balloon profile measured at that time. The autocorrelation data from which this brightness temperature spectrum is derived was shown in Fig. 3.

6. Atmospheric profile inversion

Inversion of the integral relation given by (1) can be performed in a variety of ways. Previous water vapor profiling systems have dealt primarily with statistical inversion methods, as summarized by Ulaby et al. (1986). These methods establish a relationship between

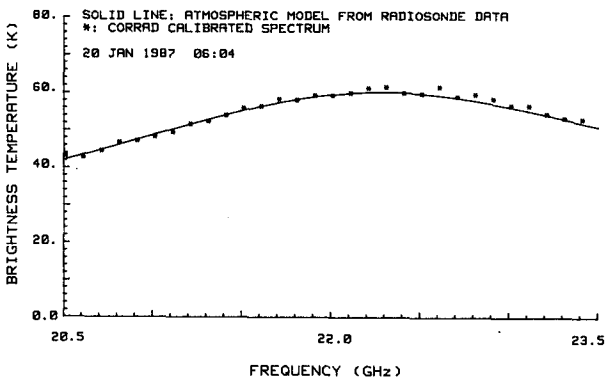

FIG. 4. Calibrated radiometer vs. balloon derived spectrum. The radiometer spectrum results from a Fourier transformation of the autocorrelation data. The balloon-derived spectrum follows from an application of the equation of radiative transfer to radiosonde profiles of the temperature, pressure, and humidity.

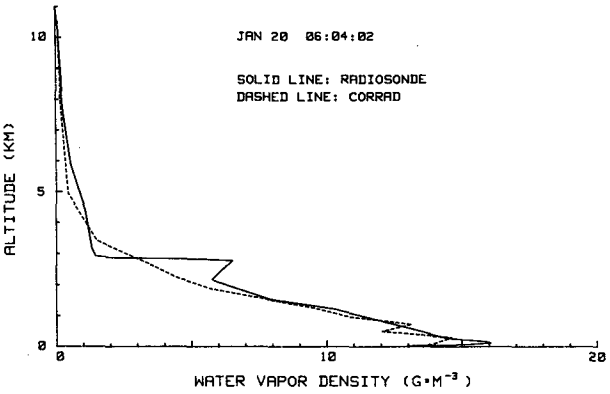

FIG. 5. Radiosonde profile vs. CORRAD inversion. The radiometer spectrum can be inverted using the integral weighting functions to estimate the vertical profile of the water vapor density which generated that spectrum. Relatively fine vertical structure such as the vapor density inversion at 2.5 km is smoothed in the radiometer estimate because of the correspondingly smooth nature of the integral weighting functions. The initial vertical lapse rate (below 2 km) is, however, tracked with much higher accuracy by the radiometer's profile.

radiometer datasets and coincident radiosonde profiles, then extrapolate that relationship to other radiometer datasets. This approach is well suited to measurement programs in which the number of independent radiometer measurements is significantly less than the number of altitude pixels in the profile estimate. It reduces the instabilities inherent in an underconstrained inversion by forcing a priori behavior on the profile estimates in the form of the original radiosonde profile shapes. One problem with this approach is that estimates of anomalous profiles—those not represented by the original database of profiles—tend to be biased toward the norm. However, it is often specifically these anomalies which are of interest to the atmospheric scientist.

The CORRAD hardware specifications listed in Table 2 illustrate the volume of data provided by the sensor. Thirty-one independent frequency bins are sampled between 20.5 and 23.5 GHz. For this reason, a more direct inversion of the radiative transfer integral equation is possible. Equation (1) is first discretized into the following matrix equation:

$$\mathbf{T}_B = W\boldsymbol{\rho}_v \tag{11}$$

where

$$(\mathbf{T}_B)_i = T_B(f_i); \quad f_i \text{ is the } i\text{th frequency bin}$$

$$(\boldsymbol{\rho}_v)_j = \rho_v(h_j); \quad h_j \text{ is the } j\text{th height bin}$$

$$W_{ij} = \int_{(h_j+h_{j+1})/2}^{(h_j+h_{j+1})/2} \int_{(f_i+f_{i-1})/2}^{(f_i+f_{i+1})/2} W(f, h)\,df\,dh$$

Equation (11) can then be inverted by minimum mean squared error estimation, giving

$$\hat{\rho}_v = (W^\dagger W)^{-1} W^\dagger \mathbf{T}_B \qquad (12)$$

where $\hat{\rho}_v$ is the water vapor density profile estimate and † denotes the matrix transpose operator.

The matrix inversion required in (12) is nearly singular. The inversion can be "regularized" by decoupling the rows and columns with a small noise term (Twomey 1963). The integral inversion can be further stabilized by constraining the estimated surface profile bin to match the coincident surface ground truth measurement by the technique of Lagrange multipliers.

It should be noted that the inversion procedure outlined here will also tend to bias the resulting profiles in a particular direction. This bias is due to the original linearization of the equation of radiative transfer noted in (1), which is performed by a first order Taylor expansion of the true, nonlinear relationship. The atmospheric profile about which the relationship is expanded is an a priori bias. This method of linearization, although mathematically similar in its final implimented form to statistical inversion, has an important conceptual difference. It allows for very natural exten-

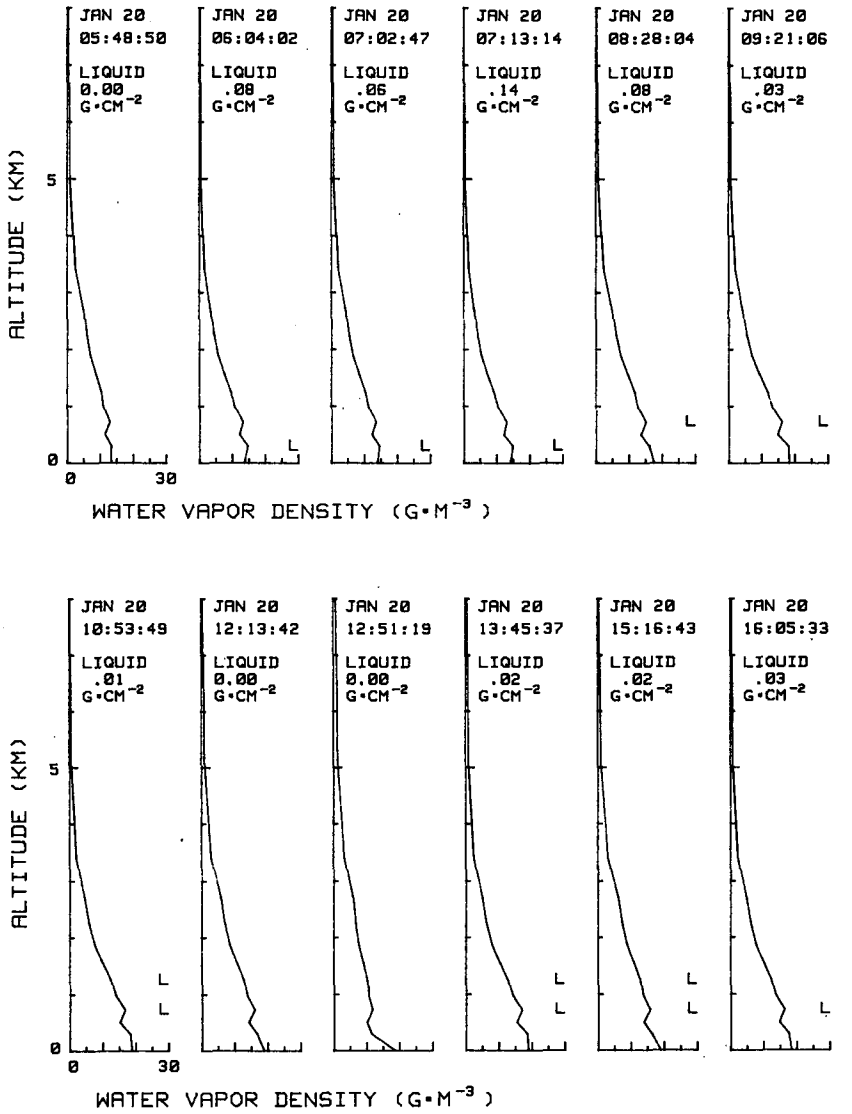

FIG. 6. The CORRAD atmospheric profile time series. Complete profiles are estimated by the radiometer at 8 min intervals. The subset shown here highlights the dynamics of the atmospheric water distribution over the course of a day. Included with the vapor density profiles are integrated liquid water content and estimated liquid water height derived from the data. Note the rise of early morning dew to form late morning cumulus at 1–1.5 km altitude.

sions of the inversion process to nonlinear, iterative forms in which the effects of initial biases are greatly reduced. This can be done by successively repeating the linearized estimation procedure, each time performing the Taylor expansion about the profile estimated by the previous iteration, until some convergence criteria is met. This is an area for future research with CORRAD.

A water vapor profile estimated during a routine radiosonde launching by the National Weather Service, along with the profile determined by that balloon, is shown in Fig. 5. The autocorrelation data and brightness temperature spectrum corresponding to this profile estimate were shown in Figs. 3 and 4, respectively.

Although nonprecipitating liquid water in the atmosphere does not exhibit resonant behavior near 22 GHz, it can be profiled indirectly from the water vapor retrieval. The brightness temperature spectrum resulting from thermal emission by the liquid can be approximated by

$$T_B(f) = T(1 - 10^{-KL}) \tag{13}$$

where

T the liquid water temperature (in K)
K $f^{1.95}e^{(1.5735-.0309T)}$, empirically derived by Benoit (1968)
L the integrated liquid water content (in g/cm^2)

The integrated nonprecipitating liquid water content is found by subtracting the brightness temperature spectrum due to the liquid from the original data spectrum which is necessary to prevent the water vapor estimate from exceeding 100% relative humidity at any altitude (assuming an average temperature profile as determined by the radiosondes). Those height bins at which it equals 100% are estimated as the liquid water (cloud) locations.

7. Experimental results

A time series of CORRAD autocorrelation datasets was taken at the National Weather Service field station in West Palm Beach, Florida on 19 and 20 January 1987. A full set of time delay measurements, requiring about 8 min, was made at 10 min intervals near sunrise and sunset and at one-half hour intervals throughout the day. A complete report of the water vapor and liquid water estimates made from this data is available from Ruf (1987). A sample is included here as Fig. 6. The letter "L" along the right edge of each plot denotes the altitude bins at which the humidity is 100%, corresponding to the probable locations of the nonprecipitating liquid water. The extremely damp surface conditions typical of a southern Florida sunrise are tracked by the high integrated liquid water content indicated.

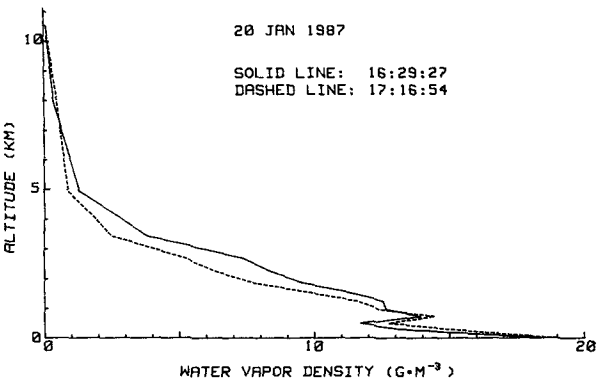

FIG. 7. CORRAD profiles before and after rainfall. Heavy afternoon showers occurred from 1655 to 1705 EDT. Note the depletion of water vapor after the rains above the cloud layer (1 km altitude).

Sunrise occurred at 0709 EDT. Later in the morning, the saturated air rises up to the 1.0–1.5 km range, and the profiles which exhibit significant liquid water content generally agree with visual cloud sightings made at the time.

One particular series of two consecutive profiles is shown in Fig. 7 as an example of the potential meteorological utility of CORRAD. The datasets were measured at 1629 and 1716 EDT on 20 January 1987. A heavy afternoon shower occurred from 1655 to 1705 EDT. The latter profile is significantly depleted of water vapor above 1.0 km. This demonstrates the potential CORRAD has for tracking dynamic weather conditions.

8. Concluding remarks

The work presented here is a preliminary verification of the viability of autocorrelation radiometry as a tool for the atmospheric sciences community. Initial results indicate that the ability to completely resolve the spectrum of the thermal emission in the region of an atmospheric resonance line (as opposed to measuring a small number of widely spaced frequency samples) tends to better constrain and, hence, stabilize the integral inversion procedure necessary to estimate vertical profiles. This, in turn, leads to a more flexible, less biased, atmospheric profiling system. In addition, the autocorrelation technique which provides this image spectrum also features improved SNR performance over alternative sampling methods because of its large predetection bandwidth.

Acknowledgments. The authors wish to thank the Hughes Aircraft Company for its donation of the front end hardware. Also, the suggestions and encouragement by E. E. Westwater, D. C. Hogg and M. T. Decker at the Environmental Research Laboratories, National Oceanic and Atmospheric Administration, Boulder, Colorado, are appreciated.

REFERENCES

Askne, J. I. H., and B. G. Skoog, 1983: Atmospheric water-vapor profiling by ground-based radiometry at 22 and 183 GHz. *IEEE Trans. Geosci. Remote Sens.*, **GE-21**(3), 320–323.

Benoit, A., 1968: signal attenuation due to neutral oxygen and water vapor, rain, and clouds. *Microwave J.*, **11**, 73–80.

Decker, M. T., E. R. Westwater and F. O. Guiraud, 1978: Experimental evaluation of ground-based microwave radiometric sensing of atmospheric temperature and water vapor profiles. *J. Appl. Meteor.*, **17**, 1788–1795.

Dicke, R. H., 1946: The measurement of thermal radiation at microwave frequencies. *Rev. Sci. Instrum.*, **17**, 268–275.

Groggins, W. B., Jr., 1967: A microwave feedback radiometer. *IEEE Trans. Aerosp. Electron. Syst.*, **AES-3**(5), 83–90.

Jones, W. L., P. G. Black, V. E. Delnore and C. T. Swift, 1981: Airborne microwave remote sensing measurements for Hurricane Allen. *Science*, **214**(4518), 274–280.

Kraus, J. D., 1966: *Radio Astronomy.* McGraw-Hill 254–255.

Page, R. M., A. Brodzinsky and R. R. Zirm, 1953: A microwave correlator. *Proc. IRE*, **41**(1), 128–131.

Papoulis, A., 1984: *Probability, Random Variables, and Stochastic Processes.* McGraw Hill, p. 265.

Rice, D. W., and K. H. Wu, 1982: Quadrature sampling with high dynamic range. *IEEE Trans. Aerosp. Electron. Syst.*, **AES-18**(6), 736–739.

Ruf, C. S., 1987: Atmospheric profiling of water vapor and liquid water with a K-Band autocorrelation radiometer. Ph.D. dissertation. University of Massachusetts, 164 pp.

Thacker, D. L., C. J. Gibbins, P. R. Schwartz and R. M. Bevilacqua, 1981: Ground based microwave observations of mesospheric H_2O in January, April, July, and September 1980. *Geophys. Res. Lett.*, **8**(10), 1059–1062.

Twomey, S., 1963: On the numerical solution of Fredholm integral equations of the first kind by the inversion of the linear equation produced by quadrature. *J. Assoc. Comput. Mach.*, **10**, 97.

Ulaby, F. T, R. K. Moore and A. K. Fung, 1981: *Microwave Remote Sensing, Active and Passive.* Vol. 1, Addison-Wesley, 256–337.

——, —— and A. K. Fung, 1986: *Microwave Remote Sensing, Active and Passive.* Vol. 3, Artech House, Inc., 1281–1329.

Vecchio, E., 1965: Technical description of sensitive correlating radiometer. Autonetics Rep. No. T-5-1422/34, Anaheim, CA.